01 Jan 2022

Additive Manufacturing of Continuous Carbon Fiber-Reinforced Sic Ceramic Composite with Multiple Fiber Bundles by an Extrusion-Based Technique

Ruoyu Chen

Adam Bratten

Joshua Rittenhouse

Ming-Chuan Leu
Missouri University of Science and Technology, mleu@mst.edu

et. al. For a complete list of authors, see https://scholarsmine.mst.edu/mec_aereng_facwork/4952

Recommended Citation

R. Chen et al., "Additive Manufacturing of Continuous Carbon Fiber-Reinforced Sic Ceramic Composite with Multiple Fiber Bundles by an Extrusion-Based Technique," *Ceramics International*, Elsevier, Jan 2022. The definitive version is available at https://doi.org/10.1016/j.ceramint.2022.11.157

Ceramics International 49 (2023) 9839–9847

Contents lists available at ScienceDirect

Ceramics International

journal homepage: www.elsevier.com/locate/ceramint

Additive manufacturing of continuous carbon fiber-reinforced SiC ceramic composite with multiple fiber bundles by an extrusion-based technique

Ruoyu Chen [a,b], Adam Bratten [b], Joshua Rittenhouse [b], Ming C. Leu [c], Haiming Wen [b,d,*]

[a] School of Metallurgical Engineering, Anhui University of Technology, Ma'anshan, Anhui, 243099, China
[b] Department of Materials Science and Engineering, Missouri University of Science and Technology, Rolla, MO, 65409, USA
[c] Department of Mechanical and Aerospace Engineering, Missouri University of Science and Technology, Rolla, MO, 65409, USA
[d] Department of Nuclear Engineering and Radiation Science, Missouri University of Science and Technology, Rolla, MO, 65409, USA

ARTICLE INFO

Keywords:
Additive manufacturing
Extrusion-based technique
SiC ceramic
Multiple continuous fiber bundle reinforcement
Core-shell structure

ABSTRACT

Due to the high cost, complex preparation process and difficulty in structural design, the traditional methods for carbon fiber-reinforced SiC ceramic composite preparation have great limitations. This paper presents a technique for the additive manufacturing multiple continuous carbon fiber bundle-reinforced SiC ceramic composite with core-shell structure using an extrusion-based technique. A conventional nozzle system was modified to print simultaneously a water-based SiC paste with continuous carbon fibers. Different levels of binder contents were investigated to optimize the stickiness, viscosity, thixotropy and viscoelasticity of the paste. After sintering, SiC whiskers were generated on the surface of fiber, which is conjectured to be due to the reaction between SiO and carbon fiber at high temperature. The continuous carbon fiber-reinforced SiC ceramic composite exhibited non-brittle fracture. The flexural strength of the additively manufactured Cf/SiC composites improved from 162 MPa with no fiber bundles to a maximum of 219 MPa with three fiber bundles.

1. Introduction

SiC ceramic matrix composites, especially continuous fiber reinforced ones, have been leading candidates in various high-temperature applications such as nuclear power and aerospace owing to their high-temperature stability, excellent mechanical properties, and low density [1,2]. Currently, the most popular method for preparing carbon fiber-reinforced SiC ceramic composite is chemical vapor infiltration (CVI) technique, which can yield high relative-density [3]. However, it is extremely expensive and time-consuming to manufacture through CVI fiber-reinforced SiC ceramic composite with a complex structure. Therefore, researchers have turned their attention from CVI technique to additive manufacturing techniques.

Among a wide variety of 3D printing techniques, extrusion-based techniques exhibit great promise in fabricating fiber reinforced ceramic composites because of their advantages in process control and low cost [4]. Xia et al. successfully prepared short carbon fiber-reinforced SiC ceramic composites with excellent mechanical strength via direct ink writing technique [5]. Lu et al. reported a new method for fabricating highly oriented short carbon fiber-reinforced SiC ceramic composite, also based on direct ink writing [6]. During printing, the short carbon fibers were highly oriented under shear force, which could be controlled by adjusting the diameter of the nozzle. The rehological behavior of the ceramic paste plays a key role in the printing process [7]. Franchin et al. optimized first the viscosity and viscoelasticity of pastes, and then used the optimized paste to print chopped carbon fiber-reinforced ceramics [8].

Compared to the short chopped carbon fiber-reinforced ceramic composites, the continuous fiber-reinforced ones possess steadiness under force, high fatigue life and large stiffness to weight ratios [9,10]. Mei et al. were the first researchers to report printing ceramics with continuous fiber reinforcement using an extrusion based technique [11]. A methyl-silsesquioxane resin was used as the ink to print, and a system similar to that for printing continuous fiber-reinforced polymer matrix composites (PMC) was adopted. However, the printer for printing continuous fiber-reinforced PMC had two feeding systems: one for ink, and the other for carbon fibers. The extrusion rate of filament is affected by many factors such as the filament feeding speed, the temperature of heating zone and the extrusion pressure, which limits the application of such systems. In addition, for these systems, the extruding tube must be heated to melt the resin during printing, which also limits its application for water-based ceramic pastes. Zhang et al. designed a needle with

* Corresponding author. Department of Materials Science and Engineering, Missouri University of Science and Technology, Rolla, MO, 65409, USA.
E-mail address: wenha@mst.edu (H. Wen).

https://doi.org/10.1016/j.ceramint.2022.11.157
Received 23 October 2022; Received in revised form 11 November 2022; Accepted 12 November 2022
Available online 14 November 2022

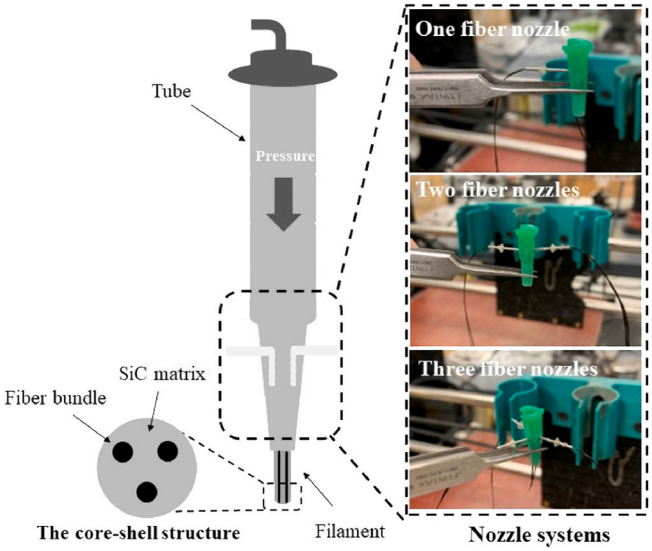

Fig. 1. Diagram illustrating the printing system and printed filament with core shell structures (left). Photographs of the nozzle systems with different numbers of fiber nozzles (right).

Table 1
Relevant printing parameters.

Pressure (Psi)	Fiber nozzle (mm)	Paste nozzle (mm)	Speed (mm/s)
35–50	0.6	1.5	1.0

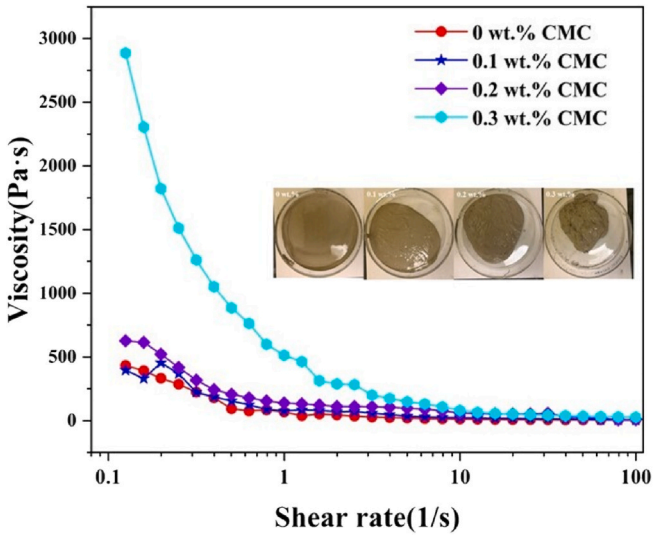

Fig. 2. Viscosity of SiC pastes with different contents of CMC.

coaxial structure to print continuous SiO_2 fiber-reinforced wave--transparent ceramics [12]. This printing system greatly simplifies the printing process.

Despite these studies, knowledge gaps clearly exist. For example, in terms of uniform extrusion of paste and fibers, there are some shortcomings in the design of the existing nozzle systems. The nozzle tilt angle affects not only the position of fibers in the filament, but also the flow rate of paste during extrusion. Moreover, the effect of the rheology of pastes on the extrusion force for fiber has not been thoroughly investigated. To address these knowledge gaps, in this study, the nozzle tilt angle in the nozzle system, including paste nozzle and fiber nozzle, and the number of fiber nozzles inserted in paste nozzle were studied

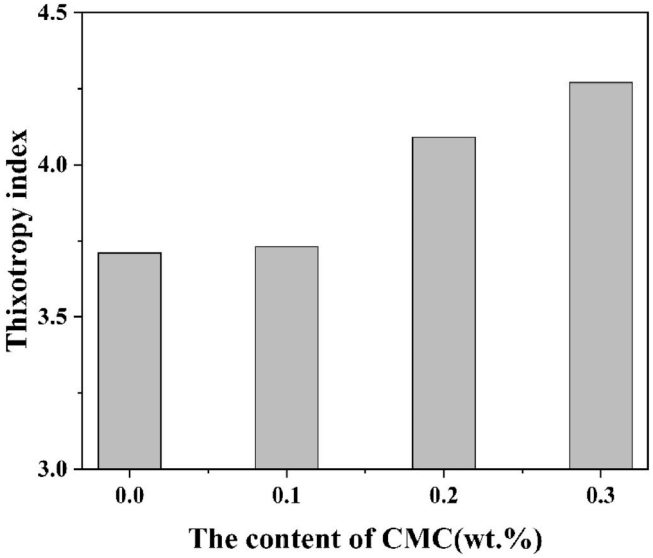

Fig. 3. Thixotropic index of SiC pastes with different contents of CMC.

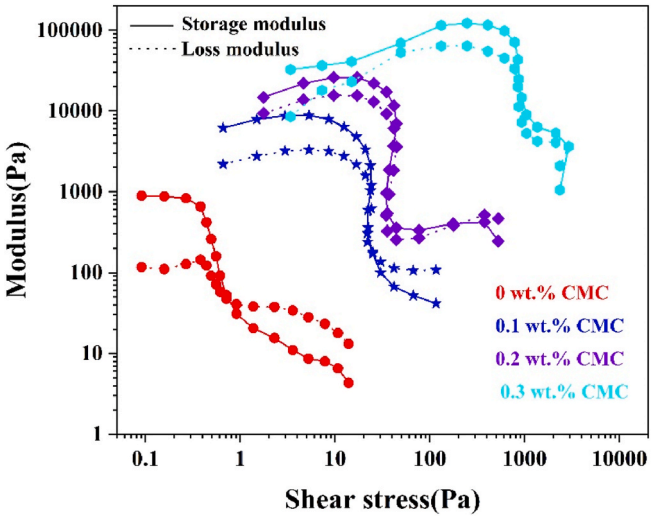

Fig. 4. Viscoelastic moduli of SiC pastes with different contents of CMC.

and optimized using a fluid field model. The rheology of SiC paste, especially the stickiness, was optimized by adjusting the amount of binder. Furthermore, the effect of fiber bundles on the mechanical properties, as well as the microstructure of continuous carbon fiber-reinforced SiC ceramic composites, was investigated.

2. Materials and methods

2.1. Paste preparation

The raw materials included SiC powders (purity ≥99%, average particle size 3.5 and 0.45 μm, Weifang Huarong Ceramic Company, China), α-Al_2O_3 powder (purity ≥99%, average particle size 0.8 μm, US Research Nanomaterials, USA) and Y_2O_3 powder (purity ≥99.9%, average particle size 0.95 μm, Atlantic Equipment Engineers, USA). Carboxymethyl cellulose (CMC) and Darvan 821A were used as binder and dispersant, respectively. The SiC paste with 78 wt% solids content was mixed in an alumina crucible containing spherical zirconia milling balls, with a ball-to-powder weight ratio of 2:1. Planetary milling was performed at 350 RPM for a total of 180 min. The solids added to the paste were composed of 95 wt% SiC, 3 wt% Al_2O_3, and 2 wt% Y_2O_3

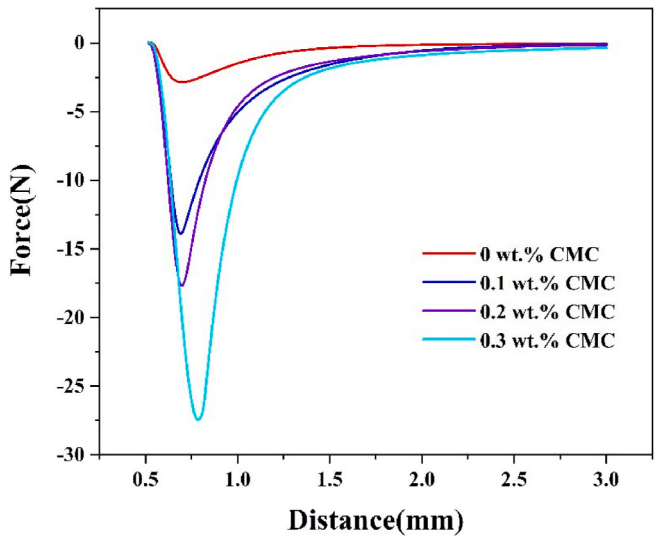

Fig. 5. Pull force of SiC pastes with different contents of CMC.

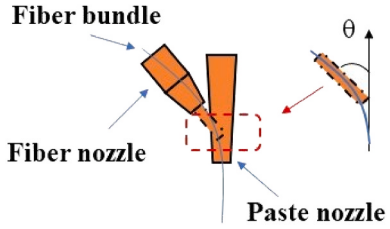

Fig. 6. Schematic of the nozzle system.

powders. Binder content ranging from 0 to 0.4 wt% was used. All components, including solid powders, binder and dispersant, as well as distilled water, were mixed by planetary ball milling for 3 h. Finally, the pH value of the SiC pastes was adjusted to 10 using NaOH solution.

2.2. 3D extrusion and sintering processes

The extrusion process was carried out by a modified commercial 3D printer (Lulzbot TAZ 6) retrofitted with a compressed air module. The structure of the 3D printer and coaxial nozzle system is shown in Fig. 1. The 3D models were constructed in Microsoft 3D builder and sliced using Simplify3D software, and then exported to generate G-code. A Python script developed in-house was used to modify the G-code to control the application of compressed air and syringe traveling path. The modified code was then executed by Simplify3D. Before printing, the continuous carbon fiber bundle was passed through the fiber nozzle. The printing parameters are shown in Table 1. During printing, the SiC paste was extruded into the paste nozzle, and the fiber bundle was covered with the SiC paste. Then the fiber bundle was co-extruded by the friction between the SiC paste and fiber bundle. After printing, samples were subsequently dried at 110 °C for 24 h. Finally, electric field-assisted liquid phase sintering was performed in a DCS-10 device (Thermal Technologies, Inc.) at 1900 °C for 15 min under Ar atmosphere. A powder bed containing SiC, Al_2O_3, and Y_2O_3 was utilized inside the crucible to inhibit volatilization at high temperature [13].

2.3. Characterization

The rheological behavior of SiC pastes was tested using a rheometer (Anton Paar MCR 102) under a continuous shear rate from 0.1 to 100 s^{-1}. The thixotropy behavior of the SiC pastes was evaluated using the thixotropy index, γ, as formulated below in equation (1) [14]:

$$\gamma = \frac{\tau_1}{\tau_2} \tag{1}$$

where τ_1 represents the viscosity at 5.012 s^{-1}, and τ_2 is the viscosity at 50.12 s^{-1}. The porosity and relative density of SiC specimens were measured by Archimedes method. Three-point flexural testing was carried out to measure the flexural strength of SiC specimens using a universal testing machine (Instron 5980). The microstructure of the printed

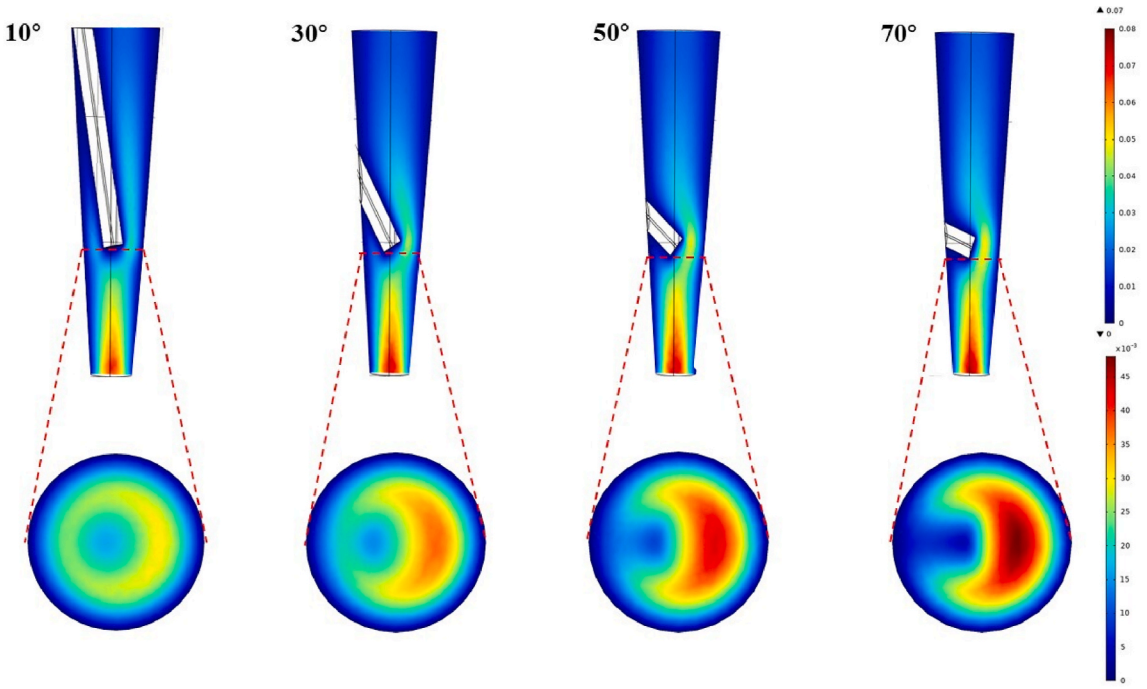

Fig. 7. Simulation results depicting the fluid speed distribution within the paste nozzle with the fiber nozzle at various angles. Bottom row: the fluid speed distribution at the bottom of the fiber nozzle.

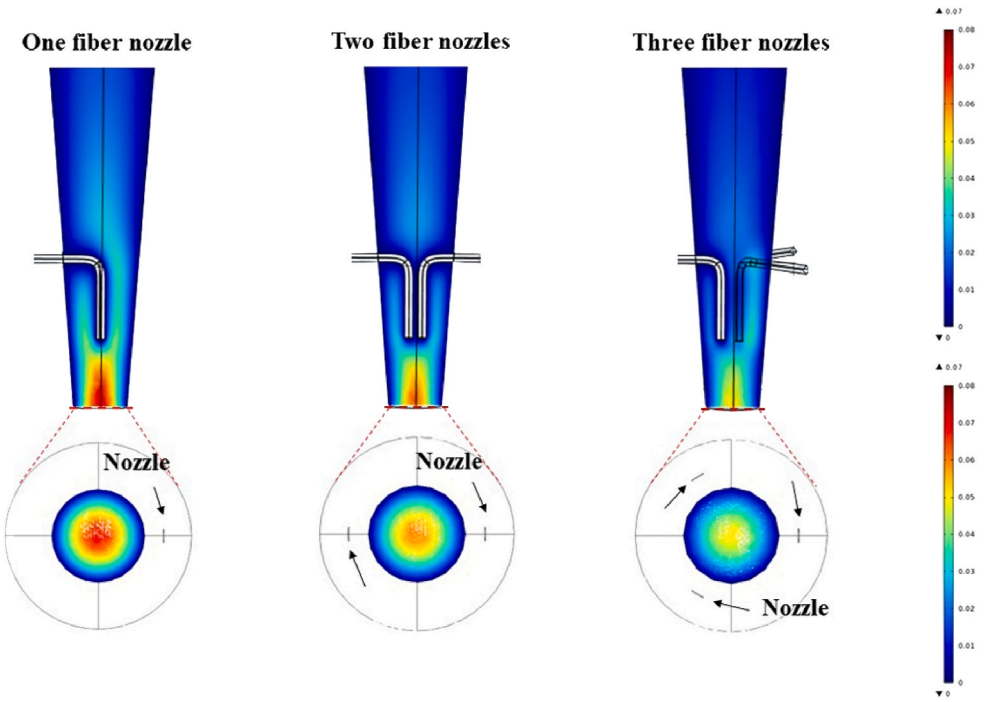

Fig. 8. Simulation results depicting the fluid speed distribution within the paste nozzle with the different number of fiber nozzle. Bottom row: the fluid speed distribution at the bottom of the paste nozzle.

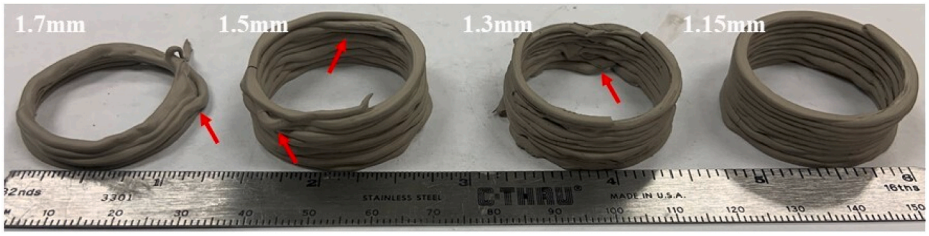

Fig. 9. Examples of SiC composite green bodies printed with layer heights from 1.7 mm (left) to 1.15 mm (right). (For interpretation of the references to colour in this figure legend, the reader is referred to the Web version of this article.)

filament and SiC specimens was analyzed using scanning electron microscopy (Tescan VEGA 3). The shear rate distribution model of the SiC paste was built using COMSOL software to analyze the effect of the position of the fiber nozzle on the shear rate of the paste during printing.

3. Results and discussion

3.1. Rheological behavior of SiC paste

For the 3D printing process, the rheological behavior of the paste has a great influence on the structure and properties of printed specimens. Printing paste should first be optimized to meet a number of key rheological requirements, including appropriate viscosity, thixotropy and viscoelasticity [15,16]. Fig. 2 shows the morphology and viscosity of the SiC pastes with different contents of CMC binder. Due to the exceedingly high viscosity of the SiC paste with 0.4 wt% CMC, results for that CMC content are not presented. As the content of CMC increased, the paste became more viscous. Meanwhile, the flowability of the SiC paste decreased significantly in the absence of shear stress. The above phenomena were caused by the increase of the interaction between CMC molecules. The Herschel-Bulkley model is used to quantify the pseudoplastic behavior of printing pastes and is formulated in equation (2) [17]:

$$\tau = \tau_0 + \kappa\gamma^n \tau = \tau_0 + \kappa\gamma^n \quad (2)$$

where τ is shear stress, τ_0 is yield stress, γ is applied shear rate, κ is the consistency index, and n is the shear-thinning index. The calculated shear-thinning index n of the SiC paste with CMC was lower than 1. Therefore, it is determined that all the as-prepared SiC pastes can be regarded as shear thinning, non-Newtonian fluids. Moreover, adding CMC enhanced the shear thinning characteristics of the SiC paste, which enabled the SiC paste to extrude smoothly and rapidly thicken after extrusion [18].

Thixotropic behavior is characterized by a decrease in the value of shear viscosity against a constant, time-independent limiting value due to constant mechanical load and the complete time-dependent recovery of the initial state upon reduction of the load [19]. It can be observed that the thixotropy of the SiC pastes was also affected by the CMC (Fig. 3). When the content of CMC increased, the recovery time of the paste viscosity decreased, which suggests that the thixotropy of the SiC pastes improved. This is likely because the rate of the disentanglement of CMC macromolecules by shearing is higher than that of re-entanglement [20]. Fig. 4 shows the storage modulus and loss modulus of the SiC pastes. It was observed that at low shear stresses, the storage modulus of the SiC pastes was higher than the loss modulus. Therefore, for the SiC pastes, the viscous properties were dominant compared to the elastic

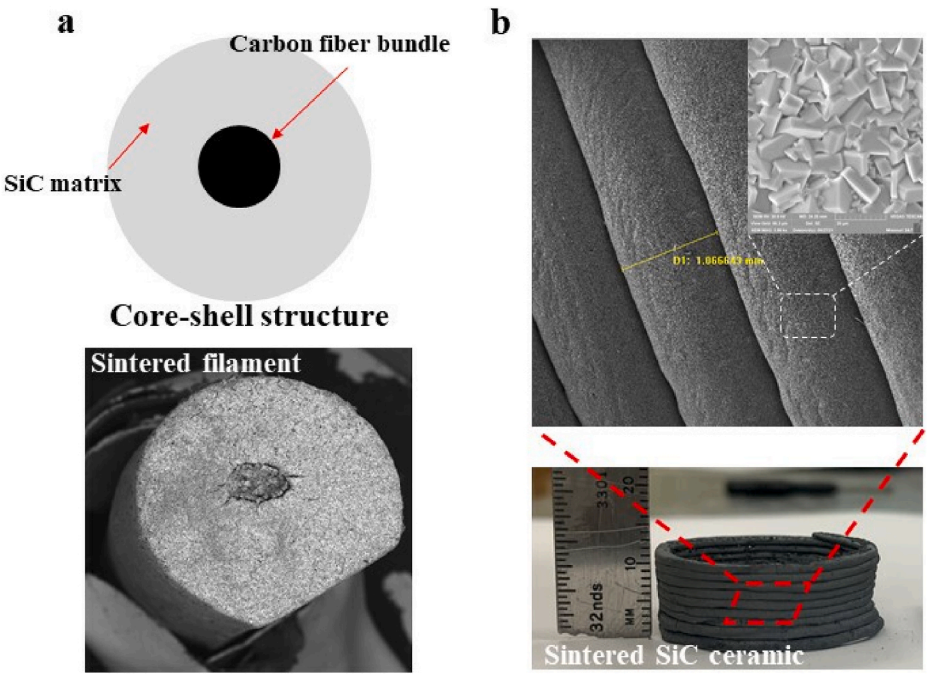

Fig. 10. a: Schematic and scanning electron micrograph of a sintered filament exhibiting the core-shell structure. b: Picture of sintered SiC specimen with secondary electron micrographs of the outer layer at low and (inset) high magnification.

properties at low shear stresses. However, when the shear stress increased, the loss modulus became greater than the storage modulus, which indicates that the behavior of the SiC pastes changed from primarily viscous to elastic. The crossover points of the storage modulus curves and loss modulus curves were established as the flow points of the SiC pastes. For 3D extrusion-based techniques, the flow points represent the points where the SiC pastes start to flow, which allow the extrusion of the SiC pastes. As the content of CMC increased from 0 to 0.3 wt%, the shear stress at the SiC paste flow points increased from 7.66×10^{-1} to 2.87×10^{3} Pa. This is attributed to the formation of a three-dimensional network of CMC molecules in the SiC pastes, and the structure of the SiC pastes with CMC was difficult to destroy.

For the 3D extrusion of paste with a continuous fiber bundle, the stickiness of the paste was one of the most important rheological factors that has frequently been ignored by researchers. While viscosity represents the resistance of a fluid to shear, stickiness describes its tendency to adhere to a surface. In this work, the force used to extrude the fibers came from the friction between the SiC pastes and the continuous fiber bundle. Therefore, the stickiness of the SiC pastes influenced the extrusion force on the fiber bundle. Stickiness is the force of adhesion that results when two surfaces are contacted with each other. Therefore, the pull force of SiC pastes was used to evaluate the stickiness of the pastes (Fig. 5) [21]. The pull force of SiC pastes increased with increasing CMC content, which indicates that the work required to overcome the attractive forces between the SiC pastes and continuous fiber bundle increased. When the SiC pastes with high amounts of CMC were used to print, the friction between the paste and continuous fiber bundle increased. The paste was extruded simultaneously with a continuous fiber bundle during the printing process, which was beneficial for improving the consistency of the structure of the printed specimens. Therefore, the SiC paste with 0.3 wt% CMC was used to print further SiC specimens with continuous fiber bundles.

3.2. Shear rate distribution model of the SiC paste during extrusion

When the fiber nozzle was inserted into the paste nozzle, an angle was formed between the two nozzles (Fig. 6). According to the existing literature [22], the nozzle tilt angle affects the position of fibers in the filament during the extrusion process. Fig. 7 displays the flow velocity model of the SiC pastes during extrusion with different types of nozzle systems. When the angle between the fiber nozzle and the paste nozzle was increased, the flow velocity of the SiC paste during the extruding process increased. The viscosity of the SiC paste decreased because of its shear-thinning properties. Viscosity is one of the main factors that influence the stickiness of pastes [23]. As the viscosity decreased, the structure of the SiC pastes broke down, resulting in a reduction of the adhesion force of the pastes. In addition, the flow velocity distribution of the SiC paste around the bottom of the fiber nozzle was extremely inhomogeneous when a large angle was used. As seen in Fig. 7, from the right to the left of the fiber nozzle bottom, the flow speed of the SiC paste decreased gradually, which had a negative influence on the uniform extrusion of the continuous fiber bundle. Because the fiber bundle was covered with the SiC paste, the inconsistent flow velocity of the paste around the fiber bundle led to inconsistency in the viscosity of the paste. This resulted in an inconsistency in the friction between the fiber bundle and the paste. In addition, the flow velocity of the paste in the center of the bottom end of the paste nozzle was much higher than at the edge when there was a large angle between the paste and fiber nozzles, which affected the shape of the printed filament. Therefore, it was determined that extruding SiC paste using the nozzle system with a small angle was more beneficial.

Moreover, based on the modeling results shown in Fig. 8, the number of fiber nozzles inserted into the side of the paste nozzles affected the flow velocity of the SiC paste. As the number of fiber nozzles increased, the flow velocity of the SiC paste decreased. Therefore, the viscosity of the SiC paste increased, which improved friction forces between the fiber bundles and the SiC paste. This is beneficial to simultaneously extrude fiber bundle and SiC paste.

3.3. Morphology and microstructure of continuous carbon fiber-reinforced SiC ceramic composite

Based on the above results, the nozzle system with a small angle was used for co-extruding the paste and fiber bundle. In order to allow for steady extrusion of composite, layer height, one of the important printing parameters, needed to be optimized [24]. The morphology of

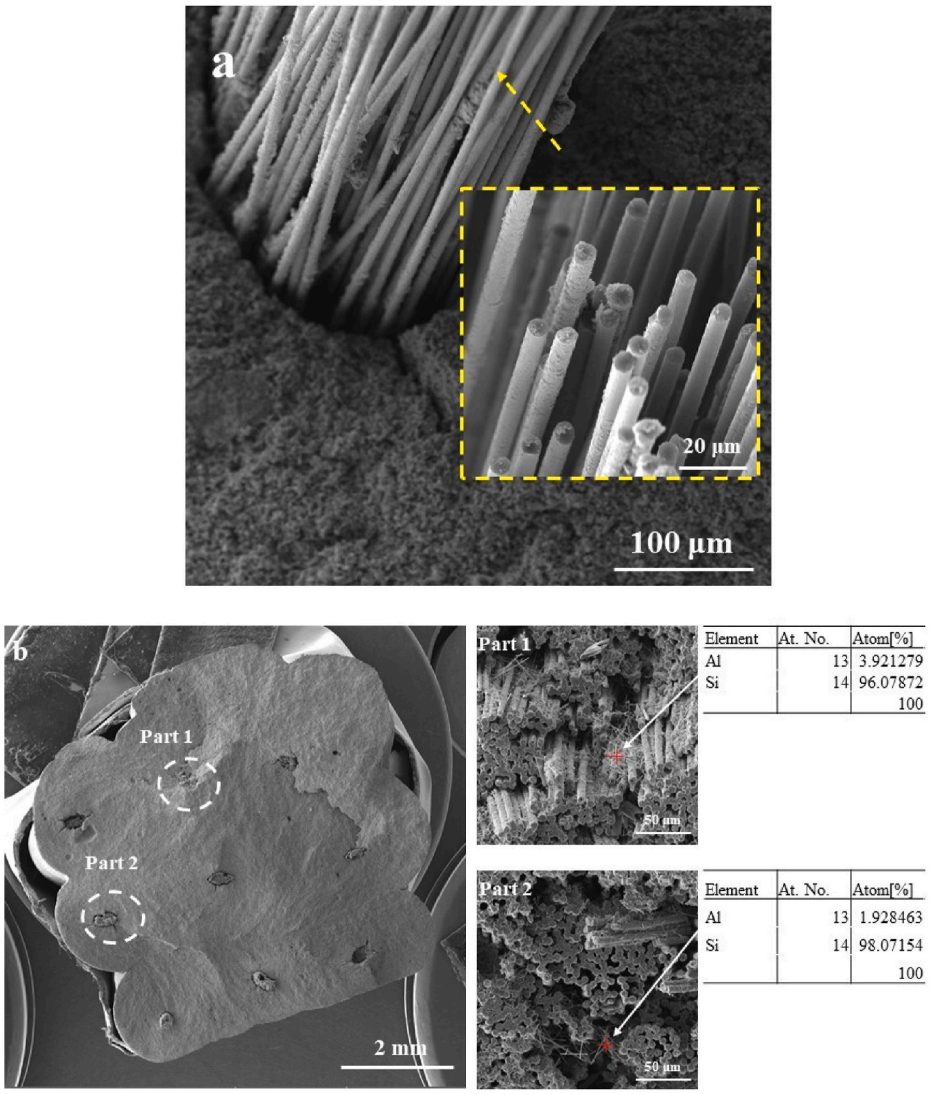

Fig. 11. Fracture surfaces of SiC ceramic composite with co-extruded fiber bundle in the (a) green state and (b) sintered state. (For interpretation of the references to colour in this figure legend, the reader is referred to the Web version of this article.)

SiC composite green bodies printed with different layer heights is shown in Fig. 8. When the layer height was large, the extruded filament bent easily, which was due to the strong adhesion between the SiC paste and continuous fiber bundle. Therefore, a reasonable reduction in the layer height was beneficial to printing filament with a stable structure. In this work, 1.15 mm layer height was used to print subsequent SiC composite green bodies.

Fig. 9 displays the morphology of sintered SiC composite specimens formed using the optimal printing parameters determined by the experiments described above. The specimens exhibited uniform shape. Because the carbon fiber bundle was extruded within the SiC matrix, a core-shell structure formed, which was retained after drying and sintering. After sintering, the layer height of the SiC composite specimens was around 1.1 mm. This was lower than the layer height in the G code model, because of 7% linear shrinkage in the height direction of the sintered specimens. As expected, the grain size of SiC increased after sintering. Meanwhile, the matrix became dense, resulting in improved strength in the sintered SiC composite specimens.

The fracture surface of representative SiC composite green bodies and sintered specimens are shown in Fig. 10. The fiber bundles distributed in the SiC matrix homogeneously. Compared to that in the green body, the surface of the fibers in the sintered specimens was rough. Moreover, interestingly, whiskers grew on the surface of the carbon fibers during sintering (Fig. 11). The main element measured using energy dispersive x-ray spectroscopy (EDS) was Si. Because EDS is known to have poor accuracy in measuring C, it is deduced that the generated whiskers were SiC [25]. At high temperatures, SiC reacted with sintering additives (Al_2O_3 and Y_2O_3) or the thin oxide layer present on SiC powder particles to form SiO gas (Equations (3)–(5)) [26,27]. Due to the presence of gaps between the fiber bundle and matrix, the gas generated may have infiltrated the fiber bundle and then reacted with carbon fibers to form SiC whiskers (Equation (6)) [28]. Some SiO_2 oxide layer may have also evaporated and reacted with carbon fibers to form SiC whiskers (Equation (7)) [28].

$$SiC_{(s)} + Al_2O_{3(s)} \rightarrow Al_2O_{(g)} + SiO_{(g)} + CO_{(g)} \quad (3)$$

$$SiC_{(s)} + Y_2O_{3(s)} \rightarrow Y_2O_{(g)} + SiO_{(g)} + CO_{(g)} \quad (4)$$

$$SiC_{(s)} + 2SiO_{2(s)} \rightarrow 3SiO_{(g)} + CO_{(g)} \quad (5)$$

$$SiO_{(g)} + C_{(s)} \rightarrow SiC_{(g)} + CO_{(g)} \quad (6)$$

$$SiO_{2(g)} + 2C_{(s)} \rightarrow SiC_{(s)} + 2CO_{(g)} \quad (7)$$

However, at longer sintering times, the volatile oxide gases (SiO and SiO_2) consumed the carbon fibers, leaving behind hollow SiC columns

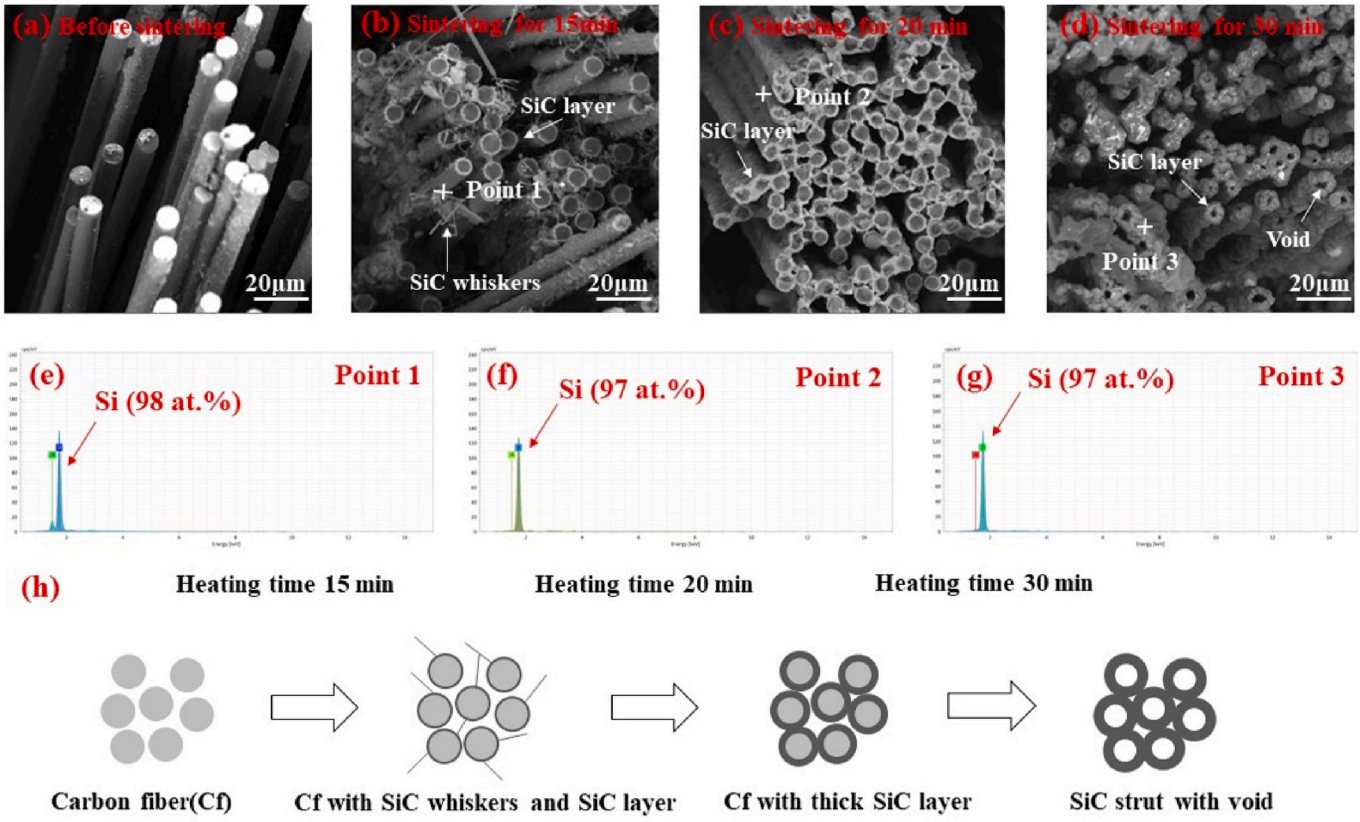

Fig. 12. (a–g) Microstructure and elemental compositions of carbon fibers in printed filaments before and after sintering with increasing hold times (h) Schematic illustrating the structure evolution of carbon fibers.

(Fig. 12), which was concomitant with reduced mechanical strength of the Cf/SiC composites. The flexural strength of specimens containing one fiber bundle decreased from 191 MPa to 159 MPa by increasing the sintering time from 15 to 30 min.

3.4. Mechanical properties of continuous carbon fiber-reinforced SiC ceramic composite

Therefore, the optimal sintering time was determined to be 15 min. The number of fiber bundles was varied from 0 to 3 to determine the effects on the mechanical properties and microstructure of the multiple continuous C_f-reinforced SiC ceramic composites (Fig. 13). The pure SiC ceramic exhibited brittle fracture, which was due to the linear propagation of cracks in the ceramic matrix. When the fibers were added into SiC matrix, the flexural strength increased significantly. As the number of fiber bundles increased, the density of the Cf/SiC composites gradually decreased. Because pores were formed between the carbon fibers as well as between the fiber bundles and SiC matrix. In contrast, the flexural strength and displacement of the Cf/SiC composites exhibited evident increases, which are attributed to fiber bridging, pull-out, and debonding phenomena [29]. Compared to the previously reported results in the literature [5,6,11,30,31], the strength values of the Cf/SiC composites in this present study are improved. The enhanced mechanical properties are attributed to the high solids content of SiC paste and multiple bundles of continuous carbon fibers used to manufacture the Cf/SiC composites. In addition, the fiber bundles were not entangled with each other and were highly orientated in the printed SiC filaments. The presence of multiple fiber bundles facilitated a more unform distribution of load in the SiC matrix and eventually resulted in improved strength and enhanced energy absorption during deformation of the Cf/SiC composites.

4. Conclusions

Multiple carbon fiber bundle-reinforced SiC ceramic composites with core-shell structure were prepared by 3D co-extrusion-based technique with high solid content SiC paste. The SiC paste with 78 wt% soild content and 0.3 wt% CMC binder exhibited outstanding rheological behavior, especially for stickiness property. The structure for the nozzle system was optimized using finite element simulation. It was notable that for printing paste with fiber, the layer height had a strong influence on the shape of printed filament as compared to other printing parameters. During sintering, the SiO gas, generated by the reaction between sintering additives or oxide layer present on SiC powders and the SiC matrix, could react with carbon fiber to form SiC whiskers. As the number of fiber bundles in the extruded filament increased, the bulk density of Cf/SiC composites decreased, however, the flexural strength of the composites was notably improved by 37% from 162 MPa to 219 MPa. In addition, the use of the field-assisted sintering technique was found to facilitate the growth of SiC whiskers on the surface of carbon fibers. Compared to the traditional manufacturing techniques for continuous carbon fiber-reinforced SiC ceramic composites, the improved 3D extrusion-based technique reported in this work exhibits low cost, strong designability and outstanding mechanical properties for the manufactured multiple carbon fiber bundles-reinforced SiC ceramic composites.

Declaration of competing interest

The authors declare that they have no known competing financial interests or personal relationships that could have appeared to influence the work reported in this paper.

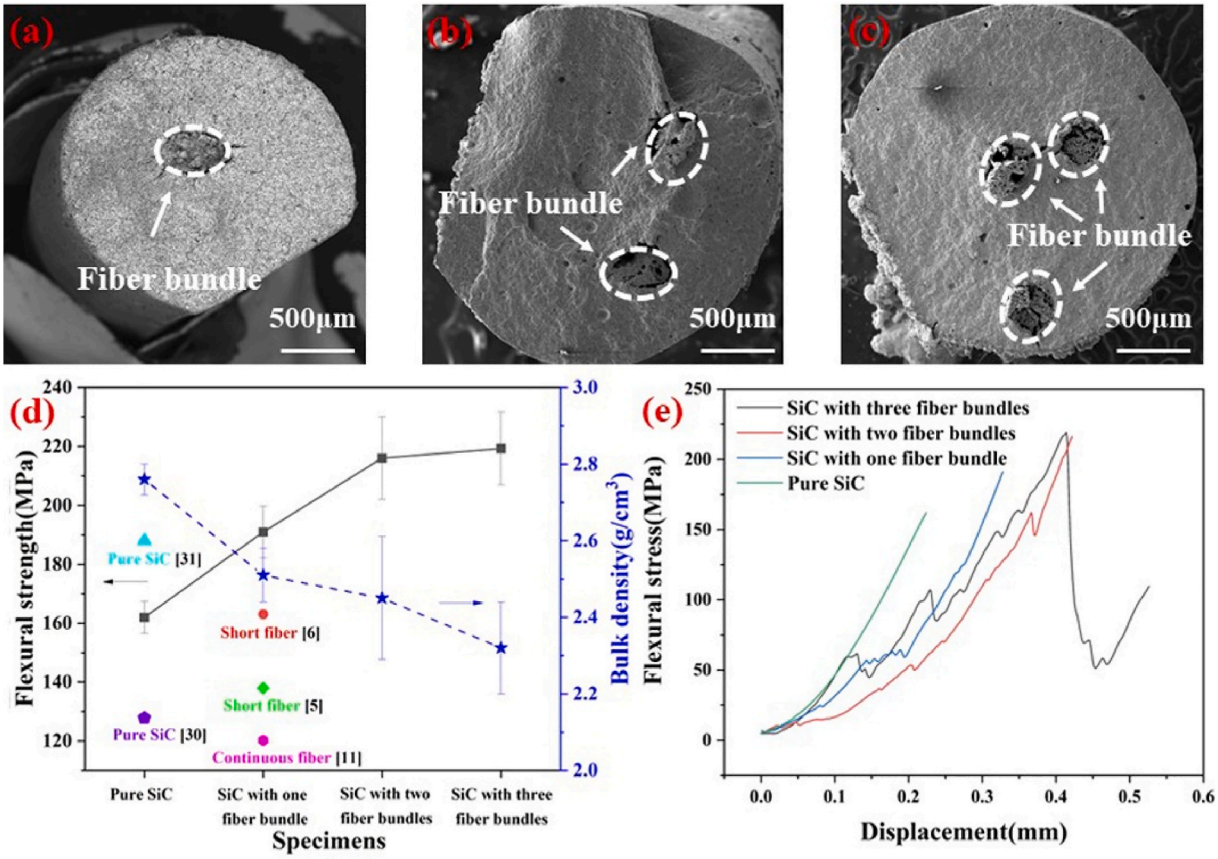

Fig. 13. (a–c) Microstructure of Cf/SiC composites containing one, two, or three continuous fiber bundles; (d) Flexural strength and bulk density of Cf/SiC composites with values for flexural strength reported in literature added (e) Flexural stress/displacement curves of Cf/SiC composites.

Acknowledgements

This study was supported by a seed grant from the Advanced Manufacturing Signature Area of Missouri University of Science and Technology. R. Chen thanks the funding for China Scholarship Council. J. Rittenhouse thanks the Office of Nuclear Energy of U.S. Department of Energy for an Integrated University Program graduate fellowship. H.M. Wen also acknowledges the U.S. Nuclear Regulatory Commission Faculty Development Program (award number NRC 31310018M0044).

References

[1] Y. Katoh, K. Ozawa, C. Shih, T. Nozawa, R.J. Shinavski, A. Hasegawa, L.L. Snead, Continuous SiC fiber, CVI SiC matrix composites for nuclear applications: properties and irradiation effects, J. Nucl. Mater. 448 (2014) 448–476, https://doi.org/10.1016/j.jnucmat.2013.06.040.

[2] S. Zhu, M. Mizuno, Y. Kagawa, Y. Mutoh, Monotonic tension, fatigue and creep behavior of SiC-fiber-reinforced SiC-matrix composites: a review, Compos. Sci. Technol. 59 (1999) 833–851, https://doi.org/10.1016/S0266-3538(99)00014-7.

[3] Y. Xu, Y. Zhang, L. Cheng, L. Zhang, J. Lou, J. Zhang, Preparation and friction behavior of carbon fiber reinforced silicon carbide matrix composites, Ceram. Int. 33 (2007) 439–445, https://doi.org/10.1016/j.ceramint.2005.10.008.

[4] G. Franchin, L. Wahl, P. Colombo, Direct ink writing of ceramic matrix composite structures, J. Am. Ceram. Soc. 100 (2017) 4397–4401. HYPERLINK "10.1111/jace.15045" \o "10.1111/jace.15045"10.1111/jace.15045.

[5] Y. Xia, Z. Lu, J. Cao, K. Miao, J. Li, D. Li, Microstructure and mechanical property of Cf/SiC core/shell composite fabricated by direct ink writing, Scripta Mater. 165 (2019) 84–88, https://doi.org/10.1016/j.scriptamat.2019.02.016.

[6] Z. Lu, Y. Xia, K. Miao, S. Li, L. Zhu, H. Nan, J. Cao, D. Li, Microstructure control of highly oriented short carbon fibres in SiC matrix composites fabricated by direct ink writing, Ceram. Int. 45 (2019) 17262–17267, https://doi.org/10.1016/j.ceramint.2019.05.283.

[7] J.A. Lewis, J.E. Smay, J. Stuecker, J. Cesarano, Direct ink writing of three-dimensional ceramic structures, J. Am. Ceram. Soc. 89 (2006) 3599–3609, https://doi.org/10.1111/j.1551-2916.2006.01382.x.

[8] G. Franchin, H.S. Maden, L. Wahl, A. Baliello, M. Pasetto, P. Colombo, Optimization and characterization of preceramic inks for direct ink writing of ceramic matrix composite structures, Materials 11 (2018) 515, https://doi.org/10.3390/ma11040515.

[9] Y. Itoh, T. Kameda, S. Suyama, K. Nagata, Material design for high strength and toughness of continuous fiber-reinforced ceramic matrix composites, J. Ceram. Soc. Jpn. 106 (1998) 1190–1195, https://doi.org/10.2109/jcersj.106.1190.

[10] Z. Hou, X. Tian, J. Zhang, D. Li, 3D printed continuous fibre reinforced composite corrugated structure, Compos. Struct. 184 (2018) 1005–1010, https://doi.org/10.1016/j.compstruct.2017.10.080.

[11] H. Mei, Y. Yan, L. Feng, K.G. Dassios, H. Zhang, L. Cheng, First printing of continuous fibers into ceramics, J. Am. Ceram. Soc. 102 (2019) 3244–3255, https://doi.org/10.1111/jace.16234.

[12] Z. Zhao, G. Zhou, Z. Yang, X. Cao, D. Jia, Y. Zhou, Direct ink writing of continuous SiO2 fiber reinforced wave-transparent ceramics, J. Adv. Ceram. 9 (2020) 1, https://doi.org/10.1007/s40145-020-0380-y.

[13] S. Baud, F. Thevenot, C. Chatillon, High temperature sintering of SiC with oxide additives: IV. Powder beds and the influence of vaporization on the behaviour of SiC compacts, J. Eur. Ceram. Soc. 23 (2003) 29–36, https://doi.org/10.1016/S0955-2219(02)00070-5.

[14] W. Jia, Y. Wang, D. Hei, R. Chen, S. Li, Effect of the amount of andalusite addition on the properties of lightweight porous reticulated materials, Construct. Build. Mater. 213 (2019) 257–264, https://doi.org/10.1016/j.conbuildmat.2019.04.032.

[15] A. Mbarki, L. Bocquet, A. Stevenson, Linking rheology and printability for dense and strong ceramics by direct ink writing, Sci. Rep. 7 (2017) 1–10, https://doi.org/10.1038/s41598-017-06115-0.

[16] S.S. Chan, M.L. Sesso, G.V. Franks, Direct ink writing of hierarchical porous alumina-stabilized emulsions: rheology and printability, J. Am. Ceram. Soc. 103 (2020) 5554–5566, https://doi.org/10.1111/jace.17305.

[17] L. Gorjan, C. Galusca, M. Sami, T. Sebastian, F. Clemens, Effect of stearic acid on rheological properties and printability of ethylene vinyl acetate based feedstocks for fused filament fabrication of alumina, Addit. Manuf. 36 (2020), 101391.

[18] S.I. Conceição, J.L. Velho, J.M.F. Ferreira, Influence of deagglomeration and carboxymethyl cellulose binders on rheological behaviour of kaolin suspensions, Appl. Clay Sci. 23 (2003) 257–264, https://doi.org/10.1016/S0169-1317(03)00125-X.

[19] T.G. Mezger, C. Sprinz, A. Green, Applied Rheology: with Joe Flow on Rheology Road, fifth ed., Anton Paar, Graz, 2018.

[20] A. Benchabane, K. Bekkour, Rheological properties of carboxymethyl cellulose (CMC) solutions, Colloid Polym. Sci. 286 (2008) 1173–1180, https://doi.org/10.1007/s00396-008-1882-2.

[21] R.C. Hoseney, J.O. Smewing, Instrumental measurement of stickiness of doughs and other foods, J. Texture Stud. 30 (1999) 123–136, https://doi.org/10.1111/j.1745-4603.1999.tb00206.x.
[22] J.M. Pappas, A.R. Thakur, M.C. Leu, X. Dong, A parametric study and characterization of additively manufactured continuous carbon fiber reinforced composites for high-speed 3D printing, Int. J. Adv. Manuf. Technol. 113 (2021) 2137–2151, https://doi.org/10.1007/s00170-021-06723-1.
[23] B. Adhikari, T. Howes, B.R. Bhandari, V. Truong, Stickiness in foods: a review of mechanisms and test methods, Int. J. Food Prop. 4 (2001) 1–33, https://doi.org/10.1081/JFP-100002186.
[24] S. Tang, L. Yang, G. Li, X. Liu, Z. Fan, 3D printing of highly-loaded slurries via layered extrusion forming: parameters optimization and control, Addit. Manuf. 28 (2019) 546–553, https://doi.org/10.1016/j.addma.2019.05.034.
[25] T.S. Aarnæs, E. Ringdalen, M. Tangstad, Silicon carbide formation from methane and silicon monoxide, Sci. Rep. 10 (2020) 1–11, https://doi.org/10.1038/s41598-020-79006-6.
[26] F.K. Van, E. Mayer, Liquid phase sintering of silicon carbide, J. Eur. Ceram. Soc. 16 (1996) 413–420, https://doi.org/10.1016/0955-2219(95)00129-8.
[27] T. Grande, H. Sommerset, E. Hagen, K. Wiik, M.A. Einarsrud, Effect of weight loss on liquid-phase-sintered silicon carbide, J. Am. Ceram. Soc. 80 (1997) 1047–1052, https://doi.org/10.1111/j.1151-2916.1997.tb02945.x.
[28] J.J. Biernacki, G.P. Wotzak, Stoichiometry of the C+ SiO_2 reaction, J. Am. Ceram. Soc. 72 (1989) 122–129, https://doi.org/10.1111/j.1151-2916.1989.tb05964.x.
[29] A. Vinci, L. Zoli, D. Sciti, J. Watts, G.E. Hilmas, W.G. Fahrenholtz, Mechanical behaviour of carbon fibre reinforced TaC/SiC and ZrC/SiC composites up to 2100° C, J. Eur. Ceram. Soc. 39 (2019) 780–787, https://doi.org/10.1016/j.jeurceramsoc.2018.11.017.
[30] X. Tian, W. Zhang, D. Li, et al., Reaction-bonded SiC derived from resin precursors by Stereolithography, Ceram. Int. 38 (2012) 589–597, https://doi.org/10.1016/j.ceramint.2011.07.047.
[31] Y. Zou, C.H. Li, Y. Tang, et al., Preform impregnation to optimize the properties and microstructure of RB-SiC prepared with laser sintering and reactive melt infiltration, J. Eur. Ceram. Soc. 40 (2020) 5186–5195, https://doi.org/10.1016/j.jeurceramsoc.2020.07.023.